crystallization papers

Crystallization and preliminary crystallographic analysis of the *Escherichia coli* tyrosine aminotransferase

**Tzu-Ping Ko,[a] Szu-Pei Wu,[b]
Wei-Zen Yang,[a] Hsin Tsai[b,c] and
Hanna S. Yuan[a]***

[a]Institute of Molecular Biology, Academia
Sinica, Taipei, Taiwan 11529, Taiwan,
[b]Department of Agricultural Chemistry, National
Taiwan University, Taipei, Taiwan, and
[c]Development Center for Biotechnology, Taipei,
Taiwan

Correspondence e-mail: hanna@sinica.edu.tw

Tyrosine aminotransferase catalyzes transamination for both dicarboxylic and aromatic amino-acid substrates. The substrate-free *Escherichia coli* tyrosine aminotransferase (eTAT) bound with the cofactor pyridoxal 5′-phosphate (PLP) was crystallized in the trigonal space group $P3_2$. A low-resolution crystal structure of eTAT was determined by molecular-replacement methods. The overall folding of eTAT resembles that of the aspartate aminotransferases, with the two identical subunits forming a dimer in which each monomer binds a PLP molecule *via* a covalent bond linked to the ε-NH$_2$ group of Lys258. Comparison of the structure of eTAT with those of the open, half-open or closed form of chicken or *E. coli* aspartate aminotransferases shows the eTAT structure to be in the open conformation.

1. Introduction

Tyrosine aminotransferase (L-tyrosine–2-oxoglutarate aminotransferase; E.C. 2.6.1.5) is a pyridoxal phosphate dependent enzyme which catalyzes the transamination reactions in the catabolic pathways for aromatic amino acids (Dietrich, 1992). In the reactions catalyzed by tyrosine aminotransferase, the α-amino group of L-tyrosine (or L-phenylalanine) is transferred to 2-oxoglutarate to yield *p*-hydroxyphenylpyruvate (or phenylpyruvate) and L-glutamate. The *E. coli* tyrosine aminotransferase (eTAT) encoded by the *tyrB* gene shares 40–50% sequence identity with aspartate aminotransferases (AATs), which constitute one of the best studied subfamilies of enzymes (Mehta *et al.*, 1989). AATs are homodimers comprised of two identical subunits, each with a molecular mass of 40–50 kDa. They catalyze the reversible transfer of an amino group specifically between dicarboxylic amino-acid substrates (aspartate or glutamate) and oxoacid substrates (oxaloacetate or 2-oxoglutarate). The crystal structures of the mitochondrial or cytosolic AATs from chicken or pig were determined more than a decade ago (Christen & Metzler, 1985; Jansonius & Vicent, 1987; Torchinsky, 1986). These structures show that each subunit of AAT contains a large domain and a small domain, and that the active site is located at the interface between these two domains. The binding of the substrate induces the enzyme to change its conformation from an open form to a closed form, in which the small domain shifts toward the active site, closing the substrate-binding pocket (Picot *et al.*, 1991; Rhee *et al.*, 1997).

AATs catalyze the transamination of dicarboxylate substrates efficiently, but are poor enzymes for aromatic substrates. On the other hand, eTAT has a broader substrate specificity: it can use not only dicarboxylate substrates but also aromatic substrates such as L-phenylalanine, L-tyrosine, L-tryptophan or the corresponding oxoacids. Here, we report the crystallization and low-resolution crystal structure of eTAT bound with a cofactor pyridoxal 5′-phosphate (PLP). Structural comparison between eTAT and the open/closed form of chicken mitochondrial AAT (McPhalen *et al.*, 1992) or half-open *E. coli* AAT (Jager *et al.*, 1994; Kamitori *et al.*, 1990; Smith *et al.*, 1989) shows that the substrate-free eTAT has a tertiary structure similar to the open form of AAT.

2. Materials and methods

The *E. coli tyrB* gene which encodes the tyrosine aminotransferase (eTAT) was isolated from the plasmid pTC29 (Liu *et al.*, 1990) and was subcloned into the expression vector pG408N under the control of λ PL promoter. The resulting plasmid was designated pTC3 (Wu *et al.*, 1998). For overexpression of the *tyrB* gene, *E. coli* N4830-1 (Pharmacia, Uppsala), which contains a temperature-sensitive λ repressor cI857, was used as the host. The pTC3-transformed cells were grown in LB medium supplemented with 1 m*M* pyridoxine and 100 µg ml^{-1} of ampicillin at 303 K. As soon as the culture reached an absorbance at 600 nm of 0.6, the temperature was shifted to 315 K and cells were permitted to grow for an

Table 1
X-ray diffraction statistics for the *E. coli* tyrosine aminotransferase.

Data collection

Resolution† (Å)	30.0–5.5/3.5
Number of observations	65956
Unique reflections	13117
Completeness† (%)	88.5
R_{merge}‡ (%)	9.3

Crystallographic refinement

Number of reflections [$F > 2\sigma(F)$]	12071
R value based on 92% data (%)	21.3
R_{free} for 8% test data set (%)	26.0
Number of non-H atoms	3080
R.m.s. deviations from ideal	
bond length (Å)	0.007
bond angle (°)	1.218
(φ, ψ) angles excluding Gly, Pro (%)	
in most-favoured regions	65.4
in additional allowed regions	30.5
Average B values (Å²)	
all atoms	56.2
range	40–73
backbone atoms (N, CA, C, O)	56.0
side-chain atoms	56.4
PLP group	43.9

† Reflections were limited to 5.5 Å along the a or b axes and 3.5 Å along the c axis. ‡ $R_{merge} = \sum_h \sum_i |I_{h,i} - \langle I_h \rangle| / \sum_h \sum_i I_{h,i}$, where $\langle I_h \rangle$ is the mean intensity of the i observations for a given reflection h.

additional 6 h to induce the overproduction of eTAT. The cellular DNA present in the crude extract was removed by precipitation with 0.2% protamine sulfate. The protein solution was then subjected to heat treatment at 327 K for 10 min. The soluble protein was purified by ammonium sulfate precipatation at 20–65% saturation, followed by chromatography using a phenyl-Sepharose CL-4B and a hydroxyapatite column. The eTAT protein washed out in the last elution step was collected and concentrated by ultrafiltration to about 5 mg ml^{-1}.

Single crystals of the eTAT protein were prepared using the hanging-drop vapour-diffusion method at room temperature. Drops containing 2.5 mg ml^{-1} eTAT, 8%(w/v) PEG 8000, 0.5 mM phenylmethyl-sulfonyl fluoride, 0.05 mM 1,4-dithiothreitol, 0.05 mM PLP and 12.5 mM phosphate buffer (pH 6.8) were equilibrated against a reservoir of 10% PEG 8000. Under these conditions, long rod-shaped crystals appeared in about three weeks. A large ($0.6 \times 0.3 \times 0.3$ mm) eTAT crystal was flash-cooled to 123 K and diffracted X-rays anisotropically to 3.2 Å resolution along the c axis and to about 5 Å in the ab plane using in-house or synchrotron X-ray radiation. Data were collected using a R-AXIS II imaging-plate detector equipped with a mirror-focused system and a Rigaku RU-300 rotating-anode generator and were processed using the *HKL* package (Otwinowski & Minor, 1997). Since the crystal diffracted anisotropically, an ellipsoidal sphere with a resolution limit of 3.5 Å at the c axis and 5.5 Å at the a and b axes was imposed on the reflection images prior to scaling. This data set contained 13117 unique reflections from 65956 observations, giving an R_{merge} of 9.3% and a completeness of 88.5% in the ellipsoidal reflection subspace. The crystal belonged to space group $P3_1$ or $P3_2$ with unit-cell dimensions $a = b = 126.6$, $c = 156.2$ Å. Assuming three TAT dimers per asymmetric unit, V_m is 2.7 Å³ Da^{-1}. The low resolution of the data was partially a consequence of the large size of the unit cell, which contained three dimers, *i.e.* 2382 (397×6) amino-acid residues, in one asymmetric unit.

Molecular-replacement calculations and subsequent crystallographic refinement

were carried out using *X-PLOR* (Brünger, 1992). A self-rotational search showed several non-crystallographic symmetry (NCS) twofold axes in the ab plane, perpendicular to the c axis, which made angles at intervals of 7.5° (0, ±7.5, ±15.0 and ±22.5°) with the a axis. The peak heights decreased as the angle increased. No significant rotational solutions were identified when the half-open or closed form of AAT were used as search models. However, cross-rotations using the open-form dimeric chicken mitochondrial AAT with all side chains included (PDB entry 7aat) as a search model yielded two strong peaks at ($\theta_1, \theta_2, \theta_3$) = (0, 91, 271°) for the first dimer and (0, 91, 254°) for the second dimer. This result was consistent with the self-rotation solutions; the molecular dyad was aligned with the a axis (0°) for the first dimer and was shifted 15.0° away from the a axis for the second dimer. Moreover, the first dimer was related to the second dimer by a twofold axis 7.5° from the a axis. The third orientation (0,90, 285°) was one of the weaker peaks in the top 20 peak list and was identified because it was also consistent with the self-rotation result. The molecular dyad for the third dimer was −15.0° away from the a axis and was related to the first dimer by a twofold axis at −7.5° from the a axis. A translational search in space group $P3_2$ with the three orientations showed peaks of 10, 7 and 4σ above the mean value, which were 6, 4 and 1.5σ higher, respectively, than the next peaks. Three dimers in the asymmetric unit were centered at (x, y, z) = (0.026, 0.053, 0), (0.667, 0.328, 0.013) and (0.327, 0.667, 0.077): almost exactly at the threefold screw axes. They gave reasonable packing in the trigonal unit cell and thus precluded a fourth dimer in the asymmetric unit. No significant translational peaks were observed when space group $P3_1$ was employed.

With the small and the large domains refined separately, rigid-body refinement of the three dimeric AAT molecules in the asymmetric unit of the $P3_2$ space group gave an R value of 0.42 for the entire data set. Upon simulated annealing with *X-PLOR* (Brünger, 1992), this heterogeneous model gave an R value of 0.23 for 92% of the data included in the refinement and an R_{free} of 0.33 for the 8% test data set. The model provided initial phase angles for the density modification (*DM*) procedure in *CCP4* (Cowtan & Main, 1996). In addition to solvent flattening and histogram matching, sixfold molecular averaging with separate large and small domains was also employed. The quality of the *DM* map was superior, mostly because of the sixfold averaging, and
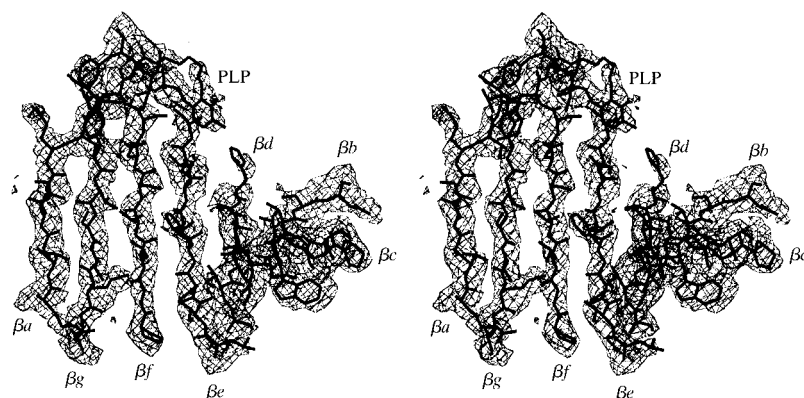

Figure 1
The stereoview of the electron-density map ($2F_o - F_c$) of *E. coli* tyrosine aminotransferase in the region of the central β-sheet of the large PLP-binding domain. The calculated phases were obtained by the molecular-replacement method using a dimeric chicken mitochondrial AAT as a model and were modified using the program *DM* (Cowtan & Main, 1996) using solvent flattening, histogram matching and sixfold averaging of the NCS-related molecules.
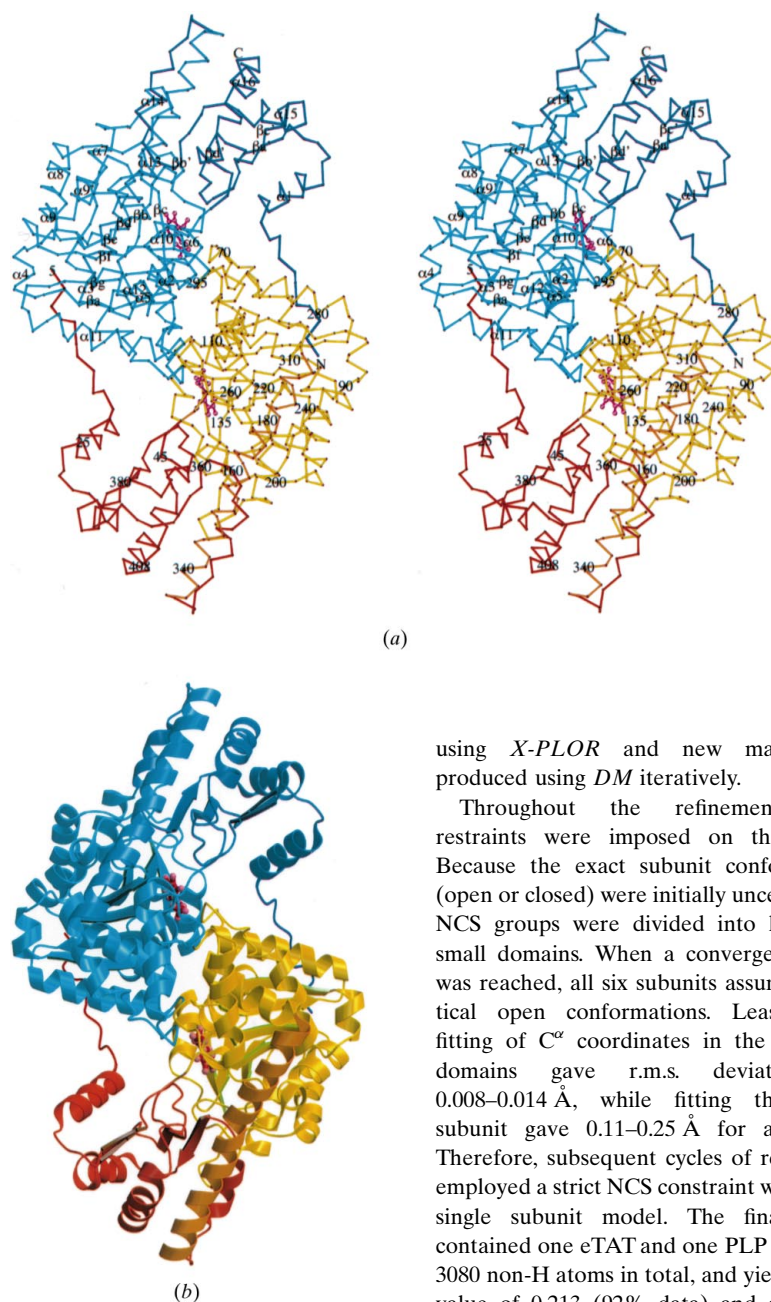
(a)

(b)

Figure 2
The structure of the dimeric *E. coli* tyrosine aminotransferase. (*a*) Stereo diagram of the C$^\alpha$ trace for the two subunits; one monomer is represented in navy and cyan, and the other monomer in red and yellow for the small and the large domains, respectively. The secondary-structural elements and the sequence numbers are indicated in the diagram for each subunit. The PLP molecule is represented as a ball-and-stick model in pink. (*b*) Ribbon diagram of the overall folding of the open-form eTAT, drawn using the program *MOLSCRIPT* (Kraulis, 1991).

clearly showed the density of the backbone, side chains and PLP molecule (see Fig. 1). The model was then modified by substituting and adjusting the side chains and inserting Gly66. The new model was refined again

using *X-PLOR* and new maps were produced using *DM* iteratively.

Throughout the refinement, NCS restraints were imposed on the model. Because the exact subunit conformations (open or closed) were initially uncertain, the NCS groups were divided into large and small domains. When a convergent model was reached, all six subunits assumed identical open conformations. Least-squares fitting of C$^\alpha$ coordinates in the six large domains gave r.m.s. deviations of 0.008–0.014 Å, while fitting the whole subunit gave 0.11–0.25 Å for all atoms. Therefore, subsequent cycles of refinement employed a strict NCS constraint with only a single subunit model. The final model contained one eTAT and one PLP molecule, 3080 non-H atoms in total, and yielded an *R* value of 0.213 (92% data) and a R_{free} of 0.260 (8% data) based on 12071 reflections having $F/\sigma(F) > 2$. No solvent molecules were included; however, the bulk-solvent setup of *X-PLOR* was used. The average temperature factor was 56.2 Å^2, with a range of 40–73 Å^2. Atoms having *B* factors larger than 70 Å^2 were located in residues 10–29 and 347–348, including helix α1 and the loop between helices α13 and α14. The r.m.s. deviations of bond lengths and bond angles from ideal values were 0.007 Å and 1.22°, respectively. Statistics are listed in Table 1.

3. Results and discussion

eTAT is numbered from 5 to 408 following the traditional adoption of the sequence

numbering of pig cytosolic AAT (Ovchinnikov *et al.*, 1973); the amino-acid residues in the opposite subunit are indicated with an asterisk. In this way, comparison of different AATs and TATs is more straightforward. The overall structure of eTAT (see Fig. 2) is similar to those of the higher animals' AAT, in which each subunit contains a small domain, a large domain and a N-terminal tail (residues 5–15). The large PLP-binding domain (residues 48–326) contains one PLP molecule, which forms an internal aldimine bond with the residue Lys258. The small domain is constituted of an N-terminal peptide (residues 16–47) and a C-terminal peptide (residues 327–408). The two domains are connected by a long α-helix (helix α13), which stretches from the centre of the large domain to the top of the small domain. The N-terminal arm extends from the small domain to wrap around the large domain, which stabilizes the dimer conformation. The topology of eTAT is similar to that of AATs, in which the large domain contains typical $\beta\alpha\beta$ motifs folded into a central seven-stranded β-sheet surrounded by three α-helices. The small domain contains two small β-sheets and five α-helices.

AATs exhibit significant rearrangement of their domain structure upon substrate binding. In the absence of substrates, AATs adopt an 'open conformation'. The binding of the substrate induces the small domain to rotate relative to the large domain, forming the 'closed conformation'. In chicken or pig AAT, the small domain rotates about 13° on changing from an open to a closed conformation (McPhalen *et al.*, 1992; Rhee *et al.*, 1997). However, in the absence of a substrate, the structure of *E. coli* AAT is in a 'half-open conformation', and the small domain rotates through 5–6° to form the closed conformation on binding a substrate (Jager *et al.*, 1994; Okamoto *et al.*, 1994; Smith *et al.*, 1989). The reasons for the reduced domain rotation for the eAAT compared with the higher animal AATs are not clear. We found that the crystal structure of eTAT best matches the open-conformation AAT. Least-squares fits were performed using the program *O* for all C$^\alpha$ atoms in one subunit, with a stringent distance cutoff of 1.0 Å, in which only the closely matched C$^\alpha$ atoms were used for fitting. In this method of fitting, the root-mean-square deviations between eTAT and AATs are 0.676 Å for the open-form chicken mAAT (PDB entry code 7aat), 0.662 Å for the unliganded eAAT (1asn) and 0.652 Å for the inhibitor-bound hexamutant eAAT (1ahx), for 132, 129 and 120 matched atom pairs, respec-
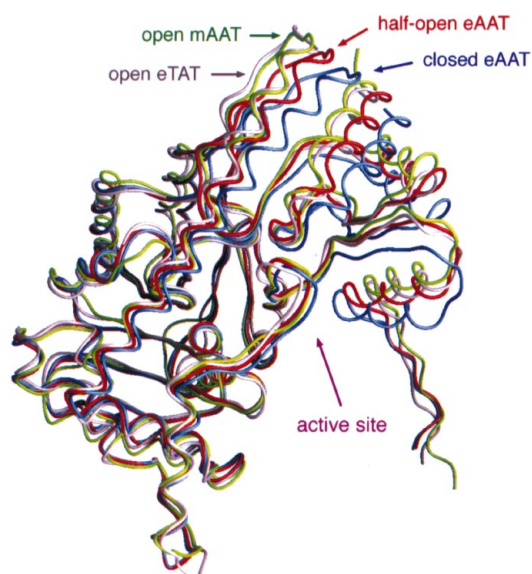
Figure 3
Superimposition of the backbones of *E. coli* tyrosine amino-transferase (eTAT) with those of aspartate aminotransferases from chicken mitochondria in the open conformation (open mAAT; McPhalen *et al.*, 1992) and *E. coli* in the half-open and closed conformations (half-open and closed eAAT; Jager *et al.*, 1994). The structure of eTAT fits well with the open-form chicken mitochondrial AAT, with an average r.m.s. difference of 1.49 Å for the C^α atoms in the small domains.

tively. The superposition of these structures is shown in Fig. 3. The backbone of eTAT fits well with that of the open-form chicken mAAT in both the large and small domains, but deviates considerably from the half-open and closed conformations of eAAT in the small domain. Specifically, for the 271 C^α atoms in the large domain, the r.m.s.d. between the eTAT model and the open mAAT, half-open eAAT and closed eAAT models are 1.38, 1.28 and 1.29 Å, respec-

tively. For the remaining 125 C^α atoms in the small domain and N-terminal segment, the r.m.s.d.s are 1.49, 2.50 and 4.35 Å, respectively

Recently, the crystal structures of the tyrosine aminotransferase from *Paracoccus denitrificans* with or without bound substrate analogues were reported (Okamoto *et al.*, 1998). These structures reveal interesting features of how a tyrosine aminotransferase accommodates an acidic as well as an aromatic substrate. A higher resolution structure of eTAT is now required to further address the question of how it is that eTAT can be an efficient enzyme for both dicarboxylate and aromatic substrates, but the highly homologous eAAT is only specific for dicarboxylate substrates.

References

Brünger, A. T. (1992). *X-PLOR Version* 3.1. *A System for X-ray Crystallography and NMR*. Yale University Press.
Christen, P. & Metzler, D. E. (1985). *Transaminases*. New York: John Wiley and Sons.
Cowtan, K. & Main, P. (1996). *Acta Cryst.* D**52**, 43–48.
Dietrich, J.-B. (1992). *Cell. Mol. Biol.* **38**, 95–114.
Jager, J., Pauptit, R. A., Sauder, U. & Jansonius, J. N. (1994). *Protein Eng.* **7**, 605–612.
Jansonius, J. N. & Vicent, M. G. (1987). *Biological Macromolecules and Assemblies*, Vol. 3, edited by F. A. Jurnak & A. McPherson, pp. 187–285. New York: John Wiley & Sons.
Kamitori, S., Okamoto, A., Hirotsu, K., Higuchi, T., Kuramitsu, S., Kagamiyama, H., Matsuura, Y. & Katsube, Y. (1990). *J. Biochem.* **108**, 175–184.
Kraulis, P. J. (1991). *J. Appl. Cryst.* **24**, 946–950.
Liu, C. C., Tu, L.-P., Chen, J.-T. & Tsai, H. (1990). *Enzymes Dependent on Pyridoxal Phosphate and Other Carbonyl Compounds as Cofactors*, edited by T. Fukui, H. Kagamiyama, K. Soda & H. Wada, pp. 579–581. Tokyo: Pergamon Press.
McPhalen, C. A., Vincent, M. G. & Jansonius, J. N. (1992). *J. Mol. Biol.* **225**, 495–517.
Mehta, P. K., Hale, T. I. & Christen, P. (1989). *Eur. J. Biochem.* **186**, 249–253.
Okamoto, A., Higuchi, T., Hirotsu, T., Kuramitsu, K. & Kagamiyama, H. (1994). *J. Biochem. (Tokyo)*, **116**, 95–107.
Okamoto, A., Nakai, Y., Hayashi, H., Hirotsu, K. & Kagamiyama, H. (1998). *J. Mol. Biol.* **280**, 443–461.
Otwinowski, Z. & Minor, W. (1997). *Methods Enzymol.* **276**, 307–326.
Ovchinnikov, Y. A., Egorov, C. A., Aldanova, N. A., Feigina, M. Y., Lipkin, V. M., Abdulaev, N. G., Grishin, E. V., Kiselev, A. P., Modyanov, N. N., Brunstein, A. E., Polyanovsky, O. L. & Nosikov, V. V. (1973). *FEBS Lett.* **29**, 31–34.
Picot, D., Sandmeier, E., Thaller, C., Vincent, M. G., Christen, P. & Jansonius, J. N. (1991). *Eur. J. Biochem.* **196**, 329–341.
Rhee, S., Silva, M. M., Hyde, C. C., Rogers, P. H., Metzler, C. M., Metzler, D. E. & Arnone, A. (1997). *J. Biol. Chem.* **272**, 17293–17302.
Smith, D., Almo, S. C., Toney, M. D. & Ringe, D. (1989). *Biochemistry*, **28**, 8161–8167.
Torchinsky, Y. M. (1986). *Vitamin B$_6$, Pyridoxal Phosphate*, Part B, edited by D. Dolphin, A. Poulson & O. Avramovic, pp. 169–221. New York: John Wiley & Sons.
Wu, S. P., Liu, C. C., Hwang, T. S., Chen, J. T. & Tsai, H. (1998). *Ann. NY Acad. Sci.* **864**, 561–4.